*Avrupa Bilim ve Teknoloji Dergisi*
*Sayı 46, S. 109-115, Ocak 2023*

***Araştırma Makalesi***

www.ejosat.com ISSN:2148-2683

*European Journal of Science and Technology*
*No. 46, pp. 109-115, January 2023*

***Research Article***

# Artificial Intelligence Based Instance-Aware Semantic Lobe Segmentation on Chest Computed Tomography Images

Beyza Sayraci*, Mahmut Ağralı, Volkan Kılıç

* İzmir Katip Çelebi University, Faculty of Engineering and Architecture, Departmant of Electrical and Electronics, İzmir, Turkey, (ORCID: 0000-0002-4059-7636, 0000-0002-5508-2854, 0000-0002-3164-1981 ), beyzasayraci@gmail.com, y210207002@ikcu.edu.tr, volkan.kilic@ikcu.edu.tr

(İlk Geliş Tarihi 24 November 2022 ve Kabul Tarihi 26 December 2022)

(**DOI:** 10.31590/ejosat.1209632)

**ATIF/REFERENCE:** Sayracı, B., Ağralı, M., & Kılıç, V., (2023). Artificial Intelligence Based Instance-Aware Semantic Lobe Segmentation on Chest Computed Tomography Images. *European Journal of Science and Technology*, (46), 109-115.

**Abstract**

The coronavirus disease (COVID-19) has taken the entire world under its influence, causing a worldwide health crisis. The most concerning complication is acute hypoxemic respiratory failure that results in fatal consequences. To alleviate the effect of COVID-19, the infected region should be analyzed before the treatment. Thus, chest computed tomography (CT) is a popular method to determine the severity level of COVID-19. Besides, the number of lobe regions containing COVID-19 on CT images helps radiologists to diagnose the findings, such as bilateral, multifocal, and multilobar. Lobe regions can be distinguished manually by radiologists, but this may result in misdiagnosis due to human intervention. Therefore, in this study, a new tool has been developed that can automatically extract lobe regions using artificial intelligence-based instance-aware semantic lobe segmentation. Convolution neural networks (CNNs) offer automatic feature extraction in the instance-aware semantic lobe segmentation task that extracts the lobe regions on CT images. In this paper, CNN-based architectures, including DeepLabV3+ with VGG-16, VGG-19, and ResNet-50, were utilized to create a benchmark for the instance-aware semantic lobe segmentation task. For further improvement in segmentation results, images were preprocessed to detect the lung region prior to lobe segmentation. In the experimental evaluations, a large-scale dataset, including 9036 images with pixel-level annotations for lung and lobe regions, has been created. DeepLabV3+ with ResNet-50 showed the highest performance in terms of dice similarity coefficient (DSC) and intersection over union (IOU) for lobe segmentation at 99.59 % and 99.19 %, respectively. The experiments demonstrated that our approach outperformed several state-of-the-art methods for the instance-aware semantic lobe segmentation task. Furthermore, a new desktop application called *LobeChestApp* was developed for the segmentation of lobe regions on chest CT images.

**Keywords:** Artificial Intelligence, Deep Learning, Instance-Aware Semantic Lobe Segmentation, COVID-19, Convolutional Neural Network.

# Akciğer Bilgisayarlı Tomografi Görüntülerinde Yapay Zekâ Tabanlı Örneğe Duyarlı Semantik Lob Segmentasyonu

**Öz**

Dünya çapında sağlık krizine neden olan Koronavirüs hastalığı (COVID-19) tüm dünyayı etkisi altına almıştır. Ölümcül sonuçlara yol açan akut hipoksemik solunum yetmezliği en çok endişe verici komplikasyondur. COVID-19'un etkisini hafifletmek için tedaviden önce enfekte olan bölge analiz edilmelidir. Bu nedenle göğüs bilgisayarlı tomografi (BT), COVID-19'a ait şiddet düzeyini belirlemek için kullanılan yaygın bir yöntemdir. Ayrıca BT görüntülerinde COVID-19 içeren lob bölgelerinin sayısı radyologların bilateral, multifokal ve multilobar gibi bulguları teşhis etmesine yardımcı olur. Lob bölgeleri radyologlar tarafından manuel olarak ayırt edilir, ancak bu uzun çalışma saatleri nedeniyle yanlış teşhislere neden olur. Bu nedenle lob bölgelerini otomatik olarak çıkarabilen yeni araçlara olan ihtiyaç artmıştır. Evrişim sinir ağları (CNN'ler), BT görüntülerinde lob bölgelerini çıkaran, örneğe duyarlı anlamsal lob segmentasyon görevinde insan hatalarını en aza indirmek için otomatik bir yaklaşım sağlar. Bu makalede, örneğe duyarlı anlamsal lob bölütleme görevinde bir kıyaslama oluşturmak için VGG-16, VGG-19 ve ResNet-50 kullanan DeepLabV3+ gibi CNN tabanlı

* Corresponding Author: beyzasayraci@gmail.com

mimariler kullanıldı. Bölütleme sonuçlarını iyileştirmek için lob bölütlemesinden önce akciğeri çıkarmada görüntülere ön işleme uygulandı. Deneysel değerlendirmeler için akciğer ve lob bölgelerini piksel düzeyinde etiketli 9036 görüntü içeren büyük ölçekli bir veri seti oluşturulmuştur. ResNet-50 kullanan DeepLabV3+, lob bölütlemede sırasıyla zar benzerlik katsayısı (DSC) ve Jaccard benzerlik katsayısı (IOU) açısından en yüksek başarımı sırasıyla ile % 99.59 ve % 99.19 olarak gösterdi. Deneyler, yaklaşımımızın, örneğe duyarlı anlamsal lob bölütleme görevi için birkaç son teknoloji yöntemden daha iyi performans gösterdi. Ayrıca, göğüs BT görüntülerinde lob bölgelerinin bölütlenmesi için *LobeChestApp* adlı yeni bir masaüstü uygulaması geliştirilmiştir.

**Anahtar Kelimeler:** Yapay Zekâ, Derin Öğrenme, Örneğe Duyarlı Anlamsal Lobe Bölütlemesi, COVID-19, Evrişimsel Sinir Ağları.

# 1. Introduction

Millions of people suffer from lung diseases, such as asthma, bronchitis, accumulation of water in the chest, shortness of breath, hydatid cyst, pleurisy, tuberculosis, and pneumonia, and four million people die from these diseases every year (Cruz, 2007). In addition, a new lung disease called COVID-19 has recently spread all over the world. To diagnose COVID-19,the real-time reverse transcription-polymerase chain reaction (RT-PCR) test detecting viral RNA via nasopharyngeal swabs has been used during this period (Wang et al., 2020). However, these tests have several drawbacks, such as requiring high-cost laboratory equipment with specialists and providing a high response time with a low detection rate. To mitigate the aforementioned issues, several approaches have been developed for diagnosing COVID-19, including biosensors, serology-based tests, and medical imaging (Giri et al., 2021). Among the approaches, medical imaging, involving X-rays, magnetic resonance imaging (MRI), and computed tomography (CT), become dominant due to their advantages in the diagnosis of COVID-19. X-rays supply poor-quality imaging, while CT and MRI offer a more detailedimage in analyzing the disease. CT is a more preferred imaging technique than MRI due to its low cost. Therefore, CT imaging has been widely used in the diagnosis of COVID-19. Over the past ten years, several studies have shown that CT imagingis necessary to assess the progress of diseases like COVID-19 (Müller, 1991). Moreover, CT imaging is considered the gold standard for analyzing morphological changes in the airways and lung parenchyma (Davis, Brody, Emond, Brumback, & Rosenfeld, 2007; Davis, Fordham, et al., 2007).

Human lungs are anatomically and functionally dividedinto five distinct sections called lobes. The left lung has two lobes, while the right lung has three lobes, as shown in Figure 1. The pulmonary lobe with the COVID-19 region on the CT image provides information about the level of the disease. However, manual identification of lobe regions is prone to human intervention leading to misdiagnosis. Therefore, an automatic system that can detect lobe regions on CT images is requiredto help radiologists during the diagnosis of COVID-19. To address this problem, artificial intelligence-based approaches, including machine learning and deep learning, have been proposed to segment lobe regions on lung images (Soomro et al., 2022). While machine learning methods are generally trained using small-scale datasets, deep learning methods, used for more complex tasks such as image classification and segmentation, require relatively large datasets to improve predictive performance (Liu & Lang, 2019).Features are manually extracted in machine learning, however,deep learning automatically extracts the features of an image. The fact that deep learning automatizes the feature extraction process leads to being preferred for medical imaging tasks (Suzuki, 2017). Deep learning utilizes neural network architectures, including convolutional neural networks (CNNs) (Akosman, Öktem, Moral, & Kılıç, 2021; Çaylı, Kılıç, Onan, & Wang, 2022; Doğan, Isık, Kılıç, & Horzum, 2022; Doğan & Kılıç, 2021; Keskin, Moral, Kılıç, & Onan, 2021; Kilic, Dogan, Kilic, & Kahyaoglu, 2022; Mercan & Kılıç, 2020; Mercan, Kılıç, & Şen, 2021; Şen et al., 2022; Yüzer, Doğan, Kılıç, & Şen, 2022), autoencoders (Palsson, Sveinsson, & Ulfarsson, 2022), recurrent neural networks (RNN) (Aydın, Çaylı, Kılıç, & Onan, 2022; Fetiler, Çaylı, Moral, Kılıç, & Onan, 2021; Keskin, Çaylı, Moral, Kılıç, & Onan, 2021; Kılıç, 2021; Mercan & Kılıç, 2020; Palaz, Doğan, & Kılıç, 2021). Among these architectures, CNNs offer promising performance forimage segmentation.

The instance-aware semantic lobe segmentation task, which labels each lobe region by enumerating between '1' and '5', provides information about COVID-19 findings, includingbilateral, multifocal, and multilobar (Simpson et al., 2020). Therefore, several approaches have been proposed for the instance-aware semantic lobe segmentation task. He *et al.* proposed a multitask multi-instance deep network ($M^2$UNet) that can classify COVID-19 and segment the lobe regions. Ferreira *et al.* introduced a fully regularized V-Net (FRV-Net) to perform the instance-aware semantic lobe segmentation task on pulmonary CT images. Tang *et al.* employed V-Net architecture for the instance-aware semantic lobe segmentation task that lung regions are extracted by threshold-based approaches.

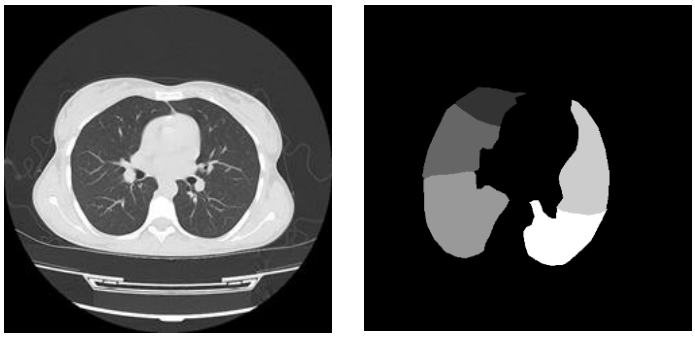

(a) (b)

*Figure 1: The lung CT image is shown in (a), while the instance-aware semantic segmented lobe CT image is given in (b).*

The approaches in (X. Chen, Zhang, & Yan, 2019; Kelei He et al., 2021a) are used a threshold-based lung extraction process before the instance-aware semantic lobe segmentation. However, the threshold-based algorithms show low performance on CT images with dense tissue.

A few datasets (Sajid, 2020; Yang et al., 2020a) are publicly available for COVID-19 segmentation or classification, however, these datasets do not contain images with lobe labels. Thus, a new dataset with pixel-level annotations for lung and lobe regions has been created. After the original images have been overlapped with corresponding lung annotations, CNN architecture was trained separately via both the original and overlapped images to analyze the effect of lung extraction on lobe segmentation. Besides, our approach has been integrated into a new user-friendly desktop application called *LobeChestApp* that performs the instance-aware semantic lobe segmentation task.

In summary, a new dataset has been collected and carried out pixel-wise annotation for lung and lobe regions on CT images. Besides, the performance of CNN architectures has been compared based on the experiments using the lung segmented and original images. Finally, our approach has been employed to develop a new desktop application called *LobeChestApp* to specify lobe regions during the diagnosis of COVID-19.

# 2. Methods

CNN architectures perform feature extraction through convolution or fully connected layers. The first layers allow CNN architectures to learn simple features in the image, while the last layers extract more complex features of the image. Popular CNN architectures, such as DeepLabV3+, VGG-16, VGG-19, and ResNet-50, for segmentation tasks were utilized to extract simple and complex features in the image. Besides, a backbone extracting simple features of the image is used in CNN architectures to increase the predicted performance.

## 2.1. DeepLabV3+

CNN-based DeepLabV3+ consists of encoder and decoder structures used for segmentation tasks (L.-C. Chen, Zhu, Papandreou, Schroff, & Adam, 2018). The encoder extracts the features of images, while the decoder reconstructs the feature maps based on the connection between two structures. The encoder extracts multi-scale features via dilated convolutions, which produce the feature map by adjusting the distance between kernel pixels (L.-C. Chen, Papandreou, Kokkinos, Murphy, & Yuille, 2017). To extract the features at different levels, the convolutions have different dilation rates, including 1, 6, 12, and 18. Each dilated convolution employs batch normalization and rectified linear units (ReLU). After the outputs of dilated convolutions are concatenated, a 1x1 convolution and an upsampling by four sequentially follow to obtain the low-level feature maps. In the decoder, a 1x1 convolution is applied to the low-level backbone feature maps extracted via CNN, like VGG-16, to reduce the number of channels. The convolution output and the feature map supplied by the encoder are concatenated to connect two structures. Next, a 3x 3 convolution and upsampling by four are used to produce the output feature map of DeepLabV3+. CNN architectures, including VGG-16, VGG-19, and ResNet50, can be utilized as a backbone of DeepLabV3+ to extract low-level features.

### 2.1.1. VGG-16 as backbone:

VGG-16 architecture is structured with five blocks containing 13 convolution layers with a 3×3 filter (Simonyan & Zisserman, 2014). After each convolution layer, a ReLu activation function exists to ensure non-linearity, which avoids acting like a single layer for sequential layers. The last layer in each block involves a 2×2 max-pooling that decreases the spatial resolution of feature maps (Das, Fime, Siddique, & Hashem, 2021). The filters of each convolution in the blocks are 64, 128, 256, 512, and 512. After the blocks, three fully connected layers perform classification tasks. However, the five blocks of VGG-16 supply low-level features for semantic segmentation architectures.

### 2.1.2. VGG-19 as backbone:

VGG-19 architecture contains five blocks with 16 convolution layers and has a small receptive field of 3x3 (Das et al., 2021). Each convolution layer follows a ReLu activation function, while a max-pooling is used in the last convolution layer of each block. After the last convolution layer, three fully connected layers follow for classification problems, but they are removed to perform the segmentation task.

### 2.1.3. ResNet-50 as backbone:

In the encoder of DeepLabV3+, ResNet-50 architecture can be utilized as a backbone to extract low-level features of images. However, the fact that ResNet-50 is deep compared to VGG-16 and VGG-19 causes a performance decrease called the degradation problem. The residual network, which involves the identity connection between the input and output of the residual blocks, is utilized in ResNet-50 to avoid the problem (Kaiming He, Zhang, Ren, & Sun, 2016). The residual blocks with three convolution layers supply more connection between the layers to improve the performance of ResNet-50. This increases the effect of the deep layers during backpropagation. ResNet-50 contains three fully connected layers later in the last convolution block for classification, but these layers were removed to feed the DeepLabV3+.

## 2.2. Instance-Aware Semantic Lobe Segmentation

A lung, shown in Figure 1, involves five lobes, including upper left, middle left, lower left, upper right, and lower right. The instance-aware semantic lobe segmentation task performs pixel-based classification for the lobes and background. The number of infected regions on each lobe provides information about the COVID-19 findings, which assists to decide the proper treatment. The

lobe segmentation task employs both original lung images and extracted lung images as input to CNN architectures. The extracted


*Figure 2: LobeChestApp after the instance-aware semantic lobe segmentation task.*

lung image increases attention to lung pixels and ignores the non-lung region, so this improves the performance of the instance-aware semantic lobe segmentation task (X. Chen et al., 2019). To perform the instance-aware semantic lobe segmentation task, DeepLabV3+ with VGG-16, VGG-19, and ResNet-50 has been trained with the collected dataset described in Section 3.1.

### 2.3. Interface: *LobeChestApp*

An artificial intelligence-based desktop application called *LobeChestApp*, given in Figure 2, was developed running DeepLabV3+ with ResNet-50 to assist radiologists in lobe segmentation during the diagnosis of COVID-19. LobeChestApp has a login screen allowing users to log in with a password to avoid unauthorized access. The main screen in *LobeChestApp* enables to upload of CT images belonging to patients via the add button. The right or left side of the main screen has an area to settle the images, such as coronal, sagittal, or axial, so all images in CT images can be analyzed through the index slider. Since the instance-aware semantic lobe segmentation task was performed on axial CT images, the segmentation process can be started after uploading them. Next, a new red button, which can display the lobe masks produced by CNN architectures, appears for analyzing lobe regions on corresponding images. The lobe masks and their corresponding images can be overlapped for better analysis of the lobe regions. Besides, the lobe masks and images can be placed on the right or left side to compare them. After visual detection of COVID-19 in the image, the users benefit from the lobe mask to specify the number of infected regions on each lobe and COVID-19 findings.

## 3. Experimental Evaluations

This section presents the collected dataset, evaluation metrics, and performance comparison of CNN architectures.

### 3.1. Dataset

The dataset is vital for CNN architectures to get a robust model. Although several datasets (Sajid, 2020; Yang et al., 2020b) used on COVID-19 classification or segmentation problems are available, as detailed in Table I, they are not suitable for the instance-aware semantic lobe segmentation task. To handle this issue, a new dataset has been created due to the lack of labeled images for the lobe region. The dataset, which includes CT images belonging to 231 cases, 86 normal and 145 diagnosed with COVID-19, has been collected with the approval of the ethics committee of Izmir Bozyaka Training and Research Hospital, Department of Radiology. The technical specifications for CT images are a matrix size of 512x512, pixel spacing of 0.82 mm, and thickness of 5 mm. CT images, which do not contain lung regions, have been ignored due to a performance decrease in CNN architectures. The lung and lobe regions on 9036 images in the dataset have been labeled via MATLAB Image Labeler App for the instance-aware semantic lobe segmentation task. The labels from ‘1’ to ‘5’ have been used for the five lobe regions in the images. Besides, the lung regions and background were labeled with ‘1’ and ‘0’ labels since the segmented lung images are employed in the instance-aware semantic lobe segmentation. Before training the CNN architectures, the min-max normalization was used to normalize the images for the preprocessing (Abdulkareem et al., 2021). Moreover, the dataset was split into training and validation subsets.

### 3.2 Evaluation Metrics

Metrics are essential to evaluate the segmentation performance between the output image of CNN architectures and the corresponding ground truth. DSC and IOU are common metrics for analyzing the performance of segmentation tasks (Geng, Zhang, Tong, & Xiao, 2019; Hofmanninger et al., 2020). The DSC indicating similarity between two binary masks, such as the output image and ground truth, is definedas follows:

*Table I: COVID-19 public datasets.*

| Dataset | Type | Images/Cases |
|---|---|---|
| PLXR (Sajid, 2020) | X-ray | 98/70 |
| CTSeg (Yang et al., 2020b) | CT | 349/216 |
| COVID-CT (Yang et al., 2020b) | CT | 812/216 |
| **Ours** | CT | **9,036/145** |

*Table II: The performance comparison for lobe segmentation.*

| Method | IOU (%) | DSC (%) |
|---|---|---|
| DeepLabV3+ (VGG-19) | 97.65 | 98.81 |
| DeepLabV3+ (VGG-16) | 97.86 | 98.92 |
| **DeepLabV3+ (ResNet-50)** | **98.74** | **99.37** |

$$DSC = \frac{2 \times TP}{2 \times TP + FN + FP} \quad (1)$$

where TP denotes true positive, the common region between the output image and the ground truth. FP means false positive, represented in the output image but does not include the region belonging to the object on the ground truth. True negative, the regions outside the union of the output image andground truth, is denoted as TN. FN stands for false negative, representing a region included within the ground truth but doesnot involve the pixels of the object in the output image. The IOU denotes the overlap ratio between the output image and ground truth as:

$$IOU = \frac{TP}{TP + FN + FP} \quad (2)$$

The greater values of the metrics indicate higher similarity between the two sets in terms of the DSC and IOU scores,which range from zero to one.

## 4. Results and Discussion

The CNN architectures DeepLabV3+, with ResNet-50, VGG-16, and VGG-19 as a backbone, have been trained and tested with the dataset introduced in Section 3.1.

Performance comparison of CNN architectures, which use the images without extracting lung regions as input, for the instance-aware semantic lobe segmentation with respect to DSC and IOU is given in **Hata! Başvuru kaynağı bulunamadı.**. The empirical results demonstrate that DeepLabV3+ with ResNet-50 outperformed other architectures with respect to DSC and IOU scores with 99.37 % and 98.74 %, respectively. DeepLabV3+ with VGG-16, which is shallower relative to VGG-19, shows the second highest result, and DeepLabV3+ (VGG-19) follows because of the degradation problem observed in deeper networks. Furthermore, the labeled lung images have been used as input for CNN architectures to analyze the impact of removing lung regions on the performance of the instance-aware semantic lobe segmentation task. The comparison of CNN architectures utilizing the labeled lung images in terms of DSC and IOU is listed in The CNN architectures DeepLabV3+, with ResNet-50, VGG-16, and VGG-19 as a backbone, have been trained. Based on the experimental results, DeepLabV3+ with ResNet-50 has shown higher performance with respect to a DSC score of 99.59 % and an IOU score of 99.19 %. Moreover, DeepLabV3+ with VGG-16 outperforms DeepLabV3+ (VGG-19).

The experimental results using the images with and without lung segmentation demonstrated that extracting the lung regions on the input images for CNN architectures increases the performance of instance-aware semantic lobe segmentation. DeepLabV3+ with ResNet-50 has shown higher performance with respect to a DSC score of 99.59 % and an IOU score of 99.19 %. Moreover, DeepLabV3+ with VGG-16 outperforms DeepLabV3+ (VGG-19). The experimental results using the images with and without lung segmentation demonstrated that extracting the lung regions on the input images for CNN architectures increases the performance of instance-aware semantic lobe segmentation. Besides, DeepLabV3+ with ResNet-50 employing labeled lung images as input for CNN architecture has been compared with recent instance-aware semantic lobe segmentation studies in terms of DSC and IOU scores in **Hata! Başvuru kaynağı bulunamadı.**.

The study in (Ferreira, Sousa, Galdran, Sousa, & Campilho, 2018) employs a relatively small-scale dataset for 3D instance-aware semantic lobe segmentation; this leads to a lack of generalization capability of the model. The fact that the approaches in (X. Chen et al., 2019; Kelei He et al., 2021b) use threshold-based algorithms in the preprocessing step to segment lung images as input of the architectures reduces the quality of lung region extraction due to dense tissue on the images. Therefore, this causes a degradation in the model performance of the instance-aware semantic lobe segmentation.

Our approach has also been employed in *LobeChestApp*, which takes 4 seconds in roughly 230 chest CT images for the instance-aware semantic lobe segmentation task. Thus, radiologists segmenting the lobe on CT images via *LobeChestApp* can decide which lobe includes the infection region after manually detecting COVID-19.

*Table III: The experimental results of the instance-aware.*

*Table IV: The comparison between our approach and state-of-the-art*

| Method | IOU (%) | DSC (%) |
|---|---|---|
| DeepLabV3+ (VGG-19) | 98.48 | 99.23 |
| DeepLabV3+ (VGG-16) | 98.98 | 99.49 |
| **DeepLabV3+ (ResNet-50)** | **99.19** | **99.59** |

*approaches for the instance-aware semantic lobe segmentation.*

| Method | IOU (%) | DSC (%) |
|---|---|---|
| $M^2$UNet **(Kelei He et al., 2021b)** | - | 78.50 |
| FRV-Net (Ferreira et al., 2018) | - | 93.00 |
| V-Net (X. Chen et al., 2019) | - | 94.17 |
| PDV-Net (Imran et al., 2020) | - | 95.00 |
| RTSU-Net (Xie, Jacobs, Charbonnier, & Van Ginneken, 2020) | 94.90 | - |
| **Our approach** | **99.19** | **99.59** |

## 5. Conclusions

In the study, CNN-based architectures have been compared for the instance-aware semantic lobe segmentation task integrated into the desktop application called LobeChestApp. Moreover, the impact of extracting the lung regions on the performance of the instance-aware semantic lobe segmentation task using CNN architectures has been analyzed. A large-scale dataset containing labeled masks for lung and lobe regions has been created using CT images with COVID-19 to train CNN architectures, including DeepLabV3+ with VGG-16, VGG-19, and ResNet-50. The highest experimental performance for lobe segmentation was achieved via DeepLabV3+ (ResNet-50) with 99.59 % and 99.19 % in terms of DSC and IOU scores. The experimental results demonstrate that our approach, which removes redundant pixels from the non-lung regions before the instance-aware semantic lobe segmentation task, is advantageous compared to several state-of-the-art methods. Therefore, DeepLabV3+ with ResNet-50 architecture has been integrated into *LobeChestApp* to segment lobe regions that assist in specifying COVID-19 findings. Thus, *LobeChestApp*, which can be used in medical centers, has the potential to help radiologists during the diagnosis of COVID-19.

## Acknowledgment

This study is supported by the Scientific and Technological Research Council of Turkey (TUBITAK) under the 2209-B Industry-Oriented Undergraduate Research Projects Support Program with project number 1139B412100452.

## References

Abdulkareem, K. H., Mohammed, M. A., Salim, A., Arif, M., Geman, O., Gupta, D., & Khanna, A. (2021). Realizing an effective COVID-19 diagnosis system based on machine learning and IOT in smart hospital environment. *IEEE Internet of Things Journal, 8*(21), 15919-15928.

Akosman, Ş. A., Öktem, M., Moral, Ö. T., & Kılıç, V. (2021). *Deep Learning-based Semantic Segmentation for Crack Detection on Marbles.* Paper presented at the 2021 29th Signal Processing and Communications Applications Conference (SIU).

Aydın, S., Çaylı, Ö., Kılıç, V., & Onan, A. (2022). Sequence-to-Sequence Video Captioning with Residual Connected Gated Recurrent Units. *J Avrupa Bilim ve Teknoloji Dergisi*(35), 380-386.

Çaylı, Ö., Kılıç, V., Onan, A., & Wang, W. (2022). *Auxiliary Classifier based Residual RNN for Image Captioning.* Paper presented at the 2022 30th European Signal Processing Conference (EUSIPCO).

Chen, L.-C., Papandreou, G., Kokkinos, I., Murphy, K., & Yuille, A. L. (2017). Deeplab: Semantic image segmentation with deep convolutional nets, atrous convolution, and fully connected crfs. *J IEEE transactions on pattern analysis, 40*(4), 834-848.

Chen, L.-C., Zhu, Y., Papandreou, G., Schroff, F., & Adam, H. (2018). *Encoder-decoder with atrous separable convolution for semantic image segmentation.* Paper presented at the Proceedings of the European conference on computer vision (ECCV).

Chen, X., Zhang, R., & Yan, P. (2019). *Feature fusion encoder decoder network for automatic liver lesion segmentation.* Paper presented at the 2019 IEEE 16th international symposium on biomedical imaging (ISBI 2019).

Cruz, A. A. (2007). *Global surveillance, prevention and control of chronic respiratory diseases: a comprehensive approach*: World Health Organization.

Das, S., Fime, A. A., Siddique, N., & Hashem, M. J. (2021). Estimation of road boundary for intelligent vehicles based on deepLabV3+ architecture. *IEEE Access, 9*, 121060-121075.

Davis, S. D., Brody, A. S., Emond, M. J., Brumback, L. C., & Rosenfeld, M. J. (2007). Endpoints for clinical trials in young children with cystic fibrosis. *Proceedings of the American Thoracic Society, 4*(4), 418-430.

Davis, S. D., Fordham, L. A., Brody, A. S., Noah, T. L., Retsch-Bogart, G. Z., Qaqish, B. F., . . . Leigh, M. W. (2007). Computed tomography reflects lower airway inflammation and tracks changes in early cystic fibrosis. *J American journal of respiratory critical care medicine, 175*(9), 943-950.

Doğan, V., Isık, T., Kılıç, V., & Horzum, N. J. (2022). A field-deployable water quality monitoring with machine learning-based smartphone colorimetry. *Analytical Methods, 14*(35), 3458-3466.

Doğan, V., & Kılıç, V. (2021). Akıllı Telefon Kullanarak Yapay Zeka Tabanlı Farenjit Tespiti: Artificial Intelligence Based Pharyngitis Detection Using Smartphone. *J Sağlık Bilimlerinde Yapay Zeka Dergisi ISSN: -, 1*(2), 14-19.

Ferreira, F. T., Sousa, P., Galdran, A., Sousa, M. R., & Campilho, A. (2018). *End-to-end supervised lung lobe segmentation.* Paper presented at the 2018 International Joint Conference on Neural Networks (IJCNN).

Fetiler, B., Çaylı, Ö., Moral, Ö. T., Kılıç, V., & Onan, A. (2021). Video captioning based on multi-layer gated recurrent unit for smartphones. *J Avrupa Bilim ve Teknoloji Dergisi*(32), 221-226.

Geng, L., Zhang, S., Tong, J., & Xiao, Z. (2019). Lung segmentation method with dilated convolution based on VGG-16 network. *J Computer Assisted Surgery, 24*(sup2), 27-33.

Giri, B., Pandey, S., Shrestha, R., Pokharel, K., Ligler, F. S., & Neupane, B. B. J. A. (2021). Review of analytical performance of COVID-19 detection methods. *Analytical bioanalytical chemistry, 413*(1), 35-48.

He, K., Zhang, X., Ren, S., & Sun, J. (2016). *Deep residual learning for image recognition.* Paper presented at the Proceedings of the IEEE conference on computer vision and pattern recognition.

He, K., Zhao, W., Xie, X., Ji, W., Liu, M., Tang, Z., Liu, J. (2021a). Synergistic learning of lung lobe segmentation and hierarchical multi-instance classification for automated severity assessment of COVID-19 in CT images. *J Pattern recognition, 113*, 107828.

He, K., Zhao, W., Xie, X., Ji, W., Liu, M., Tang, Z., . . . Liu, J. J. P. r. (2021b). Synergistic learning of lung lobe segmentation and hierarchical multi-instance classification for automated severity assessment of COVID-19 in CT images. *113*, 107828.

Hofmanninger, J., Prayer, F., Pan, J., Röhrich, S., Prosch, H., & Langs, G. (2020). Automatic lung segmentation in routine imaging is primarily a data diversity problem, not a methodology problem. *J European Radiology Experimental, 4*(1), 1-13.

Imran, A.-A.-Z., Hatamizadeh, A., Ananth, S. P., Ding, X., Tajbakhsh, N., Terzopoulos, D. J. C. M. i. B., Visualization. (2020). Fast and automatic segmentation of pulmonary lobes from chest CT using a progressive dense V-network. *8*(5), 509-518.

Keskin, R., Çaylı, Ö., Moral, Ö. T., Kılıç, V., & Onan, A. (2021). A benchmark for feature-injection architectures in image captioning. *J Avrupa Bilim ve Teknoloji Dergisi*(31), 461-468.

Keskin, R., Moral, Ö. T., Kılıç, V., & Onan, A. (2021). *Multi-GRU based automated image captioning for smartphones.* Paper presented at the 2021 29th Signal Processing and Communications Applications Conference (SIU).

Kilic, B., Dogan, V., Kilic, V., & Kahyaoglu, L. N. J. (2022). Colorimetric food spoilage monitoring with carbon dot and UV light reinforced fish gelatin films using a smartphone application. *International Journal of Biological Macromoleculesnternational Journal of Biological Macromolecules, 209*, 1562-1572.

Kılıç, V. (2021). Deep gated recurrent unit for smartphone-based image captioning. *J Sakarya University Journal of Computer Information Sciences, 4*(2), 181-191.

Liu, H., & Lang, B. J. (2019). Machine learning and deep learning methods for intrusion detection systems: A survey. *applied sciences, 9*(20), 4396.

Mercan, Ö. B., & Kılıç, V. (2020). *Deep Learning based Colorimetric Classification of Glucose with Au-Ag nanoparticles using Smartphone.* Paper presented at the 2020 Medical Technologies Congress (TIPTEKNO).

Mercan, Ö. B., Kılıç, V., & Şen, M. (2021). Machine learning-based colorimetric determination of glucose in artificial saliva with different reagents using a smartphone coupled µPAD. *J Sensors Actuators B: Chemical, 329*, 129037.

Müller, N. J. A. (1991). Clinical value of high-resolution CT in chronic diffuse lung disease. *American journal of roentgenology, 157*(6), 1163-1170.

Palaz, Z., Doğan, V., & Kılıç, V. (2021). Smartphone-based Multi-parametric Glucose Prediction using Recurrent Neural Networks. *J Avrupa Bilim ve Teknoloji Dergisi*(32), 1168-1174.

Palsson, B., Sveinsson, J. R., & Ulfarsson, M. O. J. (2022). Blind hyperspectral unmixing using autoencoders: A critical comparison. *IEEE Journal of Selected Topics in Applied Earth Observations, 15*, 1340-1372.

Sajid, N. J. M. (2020). Covid-19 patients lungs x ray images 10000.

Şen, M., Yüzer, E., Doğan, V., Avcı, İ., Ensarioğlu, K., Aykaç, A., . . . Kılıç, V. J. (2022). Colorimetric detection of H2O2 with Fe3O4@ Chi nanozyme modified µPADs using artificial intelligence. *Microchimica Acta, 189*(10), 1-11.

Simonyan, K., & Zisserman, A. (2014). Very deep convolutional networks for large-scale image recognition. *J arXiv preprint arXiv:.05645*.

Simpson, S., Kay, F. U., Abbara, S., Bhalla, S., Chung, J. H., Chung, M., . . . Ko, J. P. J. (2020). Radiological Society of North America expert consensus statement on reporting chest CT findings related to COVID-19. Endorsed by the Society of Thoracic Radiology, the American College of Radiology, and RSNA. *Journal of thoracic imaging*.

Soomro, T. A., Zheng, L., Afifi, A. J., Ali, A., Yin, M., & Gao, J. J. (2022). Artificial intelligence (AI) for medical imaging to combat coronavirus disease (COVID-19): A detailed review with direction for future research. *Artificial Intelligence Review, 55*(2), 1409-1439.

Suzuki, K. (2017). Overview of deep learning in medical imaging. *J Radiological physics technology, 10*(3), 257-273.

Wang, W., Xu, Y., Gao, R., Lu, R., Han, K., Wu, G., & Tan, W. J. J. (2020). Detection of SARS-CoV-2 in different types of clinical specimens. *323*(18), 1843-1844.

Xie, W., Jacobs, C., Charbonnier, J.-P., & Van Ginneken, B. J. I. t. o. m. i. (2020). Relational modeling for robust and efficient pulmonary lobe segmentation in CT scans. *39*(8), 2664-2675.

Yang, X., He, X., Zhao, J., Zhang, Y., Zhang, S., & Xie, P. J. (2020a). COVID-CT-dataset: a CT scan dataset about COVID-19. *arXiv preprint arXiv:.13865*.

Yang, X., He, X., Zhao, J., Zhang, Y., Zhang, S., & Xie, P. J. a. p. a. (2020b). COVID-CT-dataset: a CT scan dataset about COVID-19.

Yüzer, E., Doğan, V., Kılıç, V., & Şen, M. J. (2022). Smartphone embedded deep learning approach for highly accurate and automated colorimetric lactate analysis in sweat. *Sensors Actuators B: Chemical, 371*, 132489.